

Selective contacts and fill factor limitations in heterojunction solar cells

Luca Serenelli¹  | Luca Martini^{1,2} | Francesca Menchini^{1,2} | Massimo Izzi¹ | Giampiero de Cesare² | Giuseppe Condorelli³ | Cosimo Gerardi³ | Delfina Muñoz⁴ | Mario Tucci¹

¹ENEA, Casaccia Research Center, via Anguillarese 301, Rome, 00123, Italy

²DIET, Sapienza University of Rome, via Eudossiana 18, Rome, 00184, Italy

³Innovation, Enel Green Power, Contrada Blocco Torrazze, Zona Industriale, Catania, 95121, Italy

⁴CEA, LITEN, INES, Univ. Grenoble Alpes, 50 Avenue du lac Léman, Le Bourget-du-Lac, F-73375, France

Correspondence

Luca Serenelli, ENEA, Casaccia Research Center, via Anguillarese 301, Rome 00123, Italy.

Email: luca.serenelli@enea.it

Funding information

Horizon 2020, Grant/Award Number: 745601

Abstract

Crystalline silicon-based heterojunction (HJ) solar cells are becoming the best choice for manufacturing companies, because of the low temperature processes useful for very thin silicon wafers and the possibility to easily achieve cells efficiencies higher than 22% on n-type silicon wafers. However, the maximum cell efficiency is still limited by the typical Fill Factor (FF) value of 82%. This issue is due to several factors, some of which are sometimes underestimated, like the base contact. Indeed, a potential mismatch between the work functions of the transparent conductive oxide and the base doped layer can give rise to a small barrier against electrons collection, which is not easy to recognize when the cell FF overcomes 80%. Also a low doping efficiency of the p-type amorphous layer at the emitter side can negatively affect the FF. In this case, even if high efficiency cells are produced, their full potential is still unexploited. Thus, both selective contacts of the cell, even if apparently optimized to achieve very good results, can hide problems that limit the final cell FF and efficiency. In a previous work, an experimental method and a model to individuate hidden barriers at the base contact on n-type crystalline silicon-based HJs have been provided. In this paper, that model is applied to experimental data obtained from the characterization of both commercial and laboratory level HJ solar cells. Moreover, an easy method to recognize the presence of a barrier to the charge transport at the emitter side of the cell is illustrated.

KEYWORDS

energy barrier, fill factor, heterojunctions, selective contacts, simulations

1 | INTRODUCTION

Amorphous silicon (a-Si:H)/crystalline silicon (c-Si) heterojunction (HJ) is the technology that currently holds the record photovoltaic energy conversion efficiency for a single junction cell on silicon substrate, with the high value of 26.7%.^{1,2} This result was mainly reached thanks to the application of two concepts aiming at obtaining high efficiency: the interdigitated back contact³ and the a-Si:H/c-Si HJ

with a thin intrinsic buffer layer, originally developed by Sanyo.⁴ It has to be admitted that this kind of structure, presented for the first time in 2007 and published in 2008,⁵ still retains some problems which hinder its full exploitation at industrial level.

On the other hand, bifacial HJ technology is attracting several investors in the PV market for high efficiency cell production.⁶ During the last three years, the European H2020 AMPERE (Automated photovoltaic cell and Module industrial Production to regain and secure

This is an open access article under the terms of the Creative Commons Attribution License, which permits use, distribution and reproduction in any medium, provided the original work is properly cited.

© 2021 The Authors. Progress in Photovoltaics: Research and Applications published by John Wiley & Sons Ltd.

European Renewable Energy market) project successfully converted the 3SUN production line from amorphous/microcrystalline silicon tandem thin film modules to HJ solar cells with a maximum efficiency of 25%⁷ (22.4% on average) and a current annual capacity of 200 MWp that hopefully will be scaled up to 2 GWp.

Research from institutes and equipment producers is currently ongoing and continuously improving the cell conversion efficiency on pilot lines.⁸ Each production step is still being optimized, and new solutions and architectures are being tested, such as using half-cells to enhance the achievable power by obtaining a higher module Fill Factor (FF).⁹ This latter parameter, at cell level, is actually one of the main limiting factors for HJs. At present, typical reported FF values for HJs are indeed in the range 82–83.5%,² where the latter value is related to the actual record HJ cell with 25.1% efficiency.¹⁰ Martin Green obtained from an empirical expression a theoretical upper limit of 89% for silicon solar cells FF, only limited by Auger recombination.¹¹ However, this is not the only effect limiting the FF, as will be discussed in the following paragraphs.

In Figure 1, a typical bifacial HJ solar cell is depicted (top), and its energy band structure (as deduced from numerical simulations of the record HJ cell¹⁰) is sketched (bottom). The structure is based on a conventionally textured, n-type-doped c-Si (n-c-Si) wafer, excellently passivated on both surfaces by an intrinsic a-Si:H thin film and provided with selective contacts obtained by two doped a-Si:H films, namely (p) a-Si:H and (n) a-Si:H for the emitter and base contact, respectively.

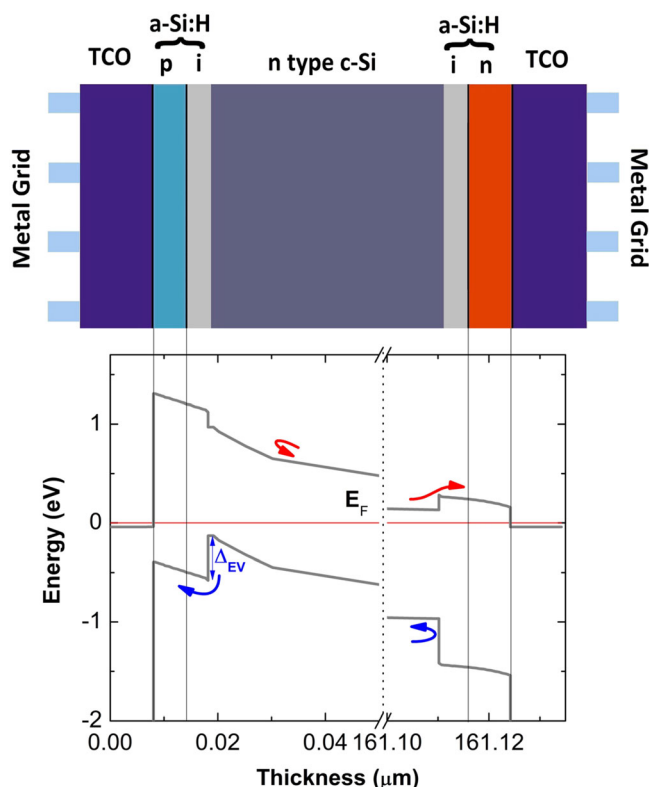


FIGURE 1 Sketch of a bifacial a-Si:H/c-Si heterojunction solar cell (top) and its band structure under dark, short circuit, and room temperature conditions (bottom) [Colour figure can be viewed at wileyonlinelibrary.com]

As specifically described elsewhere,¹² the electrons are collected by the n-c-Si/(i) a-Si:H/(n) a-Si:H/Transparent Conductive Oxide (TCO) heterostructure which forms an electron selective contact due to the valence band offset (ΔE_v) at the edge of the c-Si/a-Si:H interface. The hole collection is performed at the TCO/(p) a-Si:H/(i) a-Si:H/n-c-Si heterostructure, where the holes must cross the valence band offset at the c-Si/a-Si:H interface by jumping into the emitter, while instead the electrons are kept away by the junction electric field. The electrode contacts are ensured by films of a TCO and a screen printed silver grid on both sides, to obtain a bifacial solar cell. In this structure, the main FF limitations come from series resistance, arising from TCO lateral transport, by the specific contact resistivity between the TCO and the silver screen printed grid, and of course by the metal grid conductivity, which is usually one order of magnitude lower than that of the conventionally achieved in c-Si homojunctions, due to temperature sintering below 200°C of the screen printable silver pastes.¹³ Besides these issues, other parameters can limit the HJ FF, and they have been well addressed one by one in a previous work,¹⁴ showing how a realistic upper FF limit for this technology could be 85%. A key factor for the FF limitation is represented by the presence of barriers to charge transport which are not easily identified at Room Temperature (RT). Nevertheless, their presence can be evidenced by measuring current density/voltage (J–V) characteristics at low temperature, when a deviation from the ideal junction behavior can be observed. Such barriers can be due to different mechanisms, not always fully considered during the optimization and fabrication of devices, like energy bandgap misalignment at one or both selective contacts. Indeed, concerning the base contact, in principle, the ohmic contact on n-type c-Si is easy to produce, because of a low barrier between n-c-Si and (n) a-Si:H at the conduction band edge.¹² However, the work function of the TCO deposited above this doped layer is not always carefully considered, even because at RT it is difficult to immediately recognize any barrier issue when the cells FFs range around 80%. Considering the energy band structure of Figure 1, it can be observed that the band bending at the (n) a-Si:H/TCO interface produces an edge which induces a depletion up to the edge of c-Si wafer and then the electron flow from the base contact to the electrode experiences an undesired obstacle. This kind of bending is clearly dependent on the TCO workfunction (Φ_{TCO}): the higher the Φ_{TCO} , the higher the mismatch with the (n) a-Si:H Fermi level, and the higher the barrier to electron collection.

In a previous work,¹⁴ it has been shown how the optimal TCO work function on the base contact must range below 4.25 eV in order to avoid, at RT, any FF limitation coming from the presence of the barrier. We have also illustrated that a high doping of the a-Si:H layer can help in reducing the impact of a higher Φ_{TCO} on the FF. We have finally provided a method to reveal the presence of a hidden barrier at the base contact, by measuring the J–V characteristics of the n-c-Si/a-Si:H/(n) a-Si:H/TCO base contact alone as a function of temperature: if a limitation to the electron transport is present, the J–V characteristic of the base contact shifts from a linear (typical of an ohmic contact) to a nonlinear (similar to a Schottky barrier) curve with decreasing temperature. The analysis of the measured curves permits to define an activation energy (E_{act}) for this transition. Then we have

extrapolated a theoretical curve,¹⁴ reported as the solid line in Figure 3, which correlates E_{act} to Φ_{TCO} .

Several studies have been presented in the literature on the FF limitations due to the cell emitter side^{12,15,16} but very few on the base contact.^{17,18} We hereby carefully consider both selective contacts, their influence on the cell performances and a way to recognize if a limitation is introduced by none, one, or both of them. We detail the experimental procedure used to verify the barrier presence and apply the model to experimental data obtained from different HJ solar cells, both commercial and laboratory level.

2 | NUMERICAL SIMULATIONS

The models presented in this work have been obtained from numerical simulations of solar cells J–V characteristics at different temperatures and with different characteristics of the constituting materials, similarly to what already discussed in a previous work.¹⁴ We have followed a monodimensional description of the device along its thickness based on the homogeneity of the crystalline silicon absorber along the other two dimensions under the practical hypothesis of high-quality monocrystalline silicon. Among all the numerical simulators available to describe the carrier transport along a solar cell, intended as a stacked structure, we have preferred to use a home-made numerical simulator,¹⁹ for the sake of familiarity and good description of amorphous materials. The numerical simulator solves the Poisson, continuity, and current equations under bias condition, temperature, and light exposure, dividing the device structure in a stack of 60 sublayers: 40 of these describe the front and back side of the cell, the rest discretizes the c-Si absorber. This kind of mesh ensures a very accurate spatial description of the device in its more important parts. In particular, the description of each layer is demanded to a set of parameters, including type and concentration of dopant, electron affinity (χ), Energy gap (E_g), free carrier mobility (μ) for electrons and holes, density of states distribution, and capture cross section for both carriers. The doping of the amorphous films is simulated by varying the density of states and introducing into the forbidden gap a defect distribution centered sufficiently close to the band, to ensure a doping activation energy E_d equal to the experimentally measured one. Numerical solutions give, in each layer and at each temperature and illumination, the density of free and trapped carriers and the values of electric field and potential. Generation and recombination rates are calculated according to the Shockley–Hall–Read theory. The front and back contacts are simulated by two metals, with

no variation of the free carriers imposed.¹⁹ To simplify the description, the density of states at the interface between the a-Si:H buffer layer and c-Si is integrated along the thickness of the buffer layer and then reported as D_{it} . More details can be found in Martini et al.¹⁴ In this work, the same numerical simulator has been used to describe the emitter side behavior as a function of temperature for different doping concentration of the (p) a-Si:H layer. The most relevant properties of any material used in the device simulations, such as E_g , μ , χ , optical absorptions and refractive indexes are deduced from experimental measurements and are listed in Table 1.

3 | EXPERIMENTAL AND METHOD

3.1 | Method to investigate the base contact

As already mentioned in the introduction and described in detail elsewhere,¹⁴ it is possible to evidence the presence of a barrier at the base contact of a HJ by analyzing several J–V dark characteristics measured at different temperatures. Figure 2 shows the curve bundle relative to the base contact of two HJ cells. It can be seen that at RT the characteristic is linear, which is typical of an ohmic contact. As the temperature lowers, however, the characteristic turns to a nonlinear curve, and the effect becomes more and more pronounced with the decrease of temperature, revealing a temperature-activated process for which an activation energy (E_{act}) can be individuated. As explained, this effect is the evidence of a barrier at the electron selective contact, due to a nonideal band alignment between n-doped a-Si:H and TCO. At RT, the presence of this barrier is almost “hidden” in cells that have an overall FF above 80%.

To derive the activation energy of the transition from nonlinear to linear behavior, we have collected the current density values for each curve at a specific voltage, in the moderate forward bias range. The chosen voltage corresponds to the normal working condition of a HJ solar cell at RT, when the current density is around 37 mA/cm². The Arrhenius plot of the data (insets in Figure 2) allows extracting the E_{act} value from the slope of the linear fit of the high-temperature values.

3.2 | Cryogenic measurements

Dark and light measurements of the J–V characteristics of complete cells and selective contacts have been carried out in a cryogenic

TABLE 1 Experimentally determined parameters for the materials used in the numerical simulations of the solar cells (see text for details)

Material	E_g (eV)	$\mu_{n,p}$ (cm ² /V·s)	χ (eV)	$E_{d-n,p}$ (eV)	Thickness
c-Si	1.124	1417–470	4.05	0.175	160 μm
(i) a-Si:H	1.72	1–0.1	3.9		5 nm
(n) a-Si:H	1.72	1–0.1	3.9	0.17	15 nm
(p) a-Si:H	1.72	1–0.1	3.9	0.42	5 nm

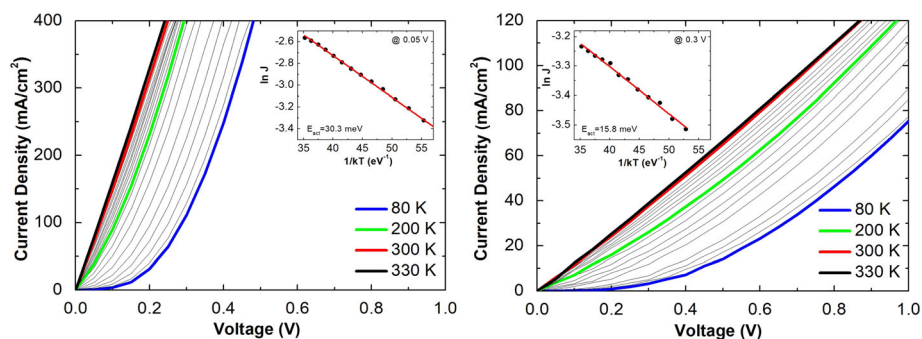


FIGURE 2 Bundle of J–V characteristics of the base contact of (left) cell A and (right) cell F of Table 2, measured at different temperatures. A transition from a linear to a nonlinear shape with decreasing temperature is evident. The insets show the Arrhenius plots of J values collected at the specified voltage, and the red line is a linear fit of the high-temperature values, which slope corresponds to the activation energy E_{act} [Colour figure can be viewed at wileyonlinelibrary.com]

TABLE 2 Details on the different ITO layers deposited on the investigated samples

Sample	Base contact ITO	Front contact ITO
Cell A	Pulsed DC sputtered type 1, 200°C	Pulsed DC sputtered type 1, 200°C
Cell B	DC sputtered type 3, RT	DC sputtered type 3, RT
Cell C	DC sputtered type 3, 180°C	DC sputtered type 3, RT
Cell D	DC sputtered type 2, 200°C	DC sputtered type 2, 200°C
Cell E	RF sputtered type 3, 180°C	RF sputtered type 3, RT
Cell F	RF sputtered type 4, 180°C	-

Note: See text for further information.

system in the temperature range 80–330 K. The cooling has been demanded to liquid nitrogen, while a Proportional–Integral–Derivative (PID)-controlled heating system has ensured a slow temperature increase during which the J–V characteristics have been collected at steps of 10 K. A copper plate has established the thermal and electrical contact with the rear of the sample. During light measurements, the samples have been illuminated by a halogen lamp through a transparent window. The lamp light intensity has been calibrated to match the J_{sc} of the cells measured under standard AM 1.5G conditions.

3.3 | Samples preparation

The samples investigated in this work are obtained from six HJ solar cells produced in different laboratories. The samples have the basic structure sketched in Figure 1. All the cells are based on n-type 1–5 Ω/cm c-Si wafers and contain layers of (n)- and (p)-doped a-Si:H, while they differ in several aspects like the thickness and dopant concentration of the amorphous layers, the type of intrinsic buffer layer used for the c-Si surface passivation, the Indium Tin Oxide (ITO) sputtering process parameters, and the metallization. Some relevant details on the samples are reported in Table 2.

Cell A has been fabricated in a pilot line at CEA-INES. The amorphous silicon layers have been deposited by Radio Frequency Plasma Enhanced Chemical Vapor Deposition (PECVD) at 13.56 MHz in a Meyer Burger HeLiA reactor. All the doped amorphous layers have a dopant concentration higher than 10^{20} at/cm³, as obtained by secondary-ion mass spectrometry (SIMS) profiles. More details can be found elsewhere.²⁰ The total thickness of the emitter stack (intrinsic + doped amorphous silicon) is 25–30 nm, while for the base contact side the total thickness is 8–12 nm. ITO layers have been deposited on both sides of the cell by pulsed Direct Current (DC) sputtering at 200°C from a 97:3 In:Sn target and have a thickness around 70 nm (referred as type 1 in Table 2).

Cells B, C, and D precursors have been manufactured in the production line at the Enel Green Power (EGP) factory, with deposition conditions very similar to those of cell A. The dopant concentration in the amorphous films, measured by SIMS profile, is around 10^{21} at/cm³. The total thickness of the emitter stack is 20–25 nm, while the base contact stack is 10–15 nm thick. The three cells have different TCO layers: Cell D has been completed at EGP by 80 nm thick ITO films deposited on both sides by DC sputtering at 150–200°C from a 97:3 In:Sn target (type 2). The ITO layers of cells B and C have been deposited by DC sputtering at the ENEA laboratories (type 3) from a 90:10 In:Sn target. All ITO layers on the (p) a-Si:H side have been deposited at RT while, in order to investigate different combinations of TCOs, the ITO film on the base contacts has been deposited at 180°C for cell C and at RT for cell B. All the ITO layer thicknesses are around 80 nm.

Cells E and F have been both manufactured at the ENEA laboratories and contain 5-nm-thick a-SiOx:H passivation layers.²¹ The doped layers have been deposited in a three chamber 13.56 MHz PECVD system, with a thickness of about 15 nm in case of the base contact and 10 nm in the case of the emitter. The ITO layers on the base contact have been deposited by RF sputtering at 180°C for both cells, but in different sputtering systems (indicated as types 3 and 4 in Table 2, respectively). Sample F has been intentionally used as a base contact structure for reference.

All cells have been metallized by screen printing. Grid design, silver paste, and printing/curing conditions are the same for cells A and D, while they are different for each of the cells B, C, and E.

In order to characterize the base and emitter selective contacts separately, the opposite side of the HJ cells has been completely removed by applying a solution of diluted hydrofluoric acid (HF) and hydrogen peroxide (H_2O_2), which allows obtaining a clean silicon surface. The ohmic contact has been ensured by the application of a eutectic of indium and gallium (InGa) on the c-Si surface; this contact has been proven to be ohmic in the whole range of considered temperatures.

For completeness, Table 3 summarizes the photovoltaic parameters of the cells. The differences in performances are clearly related to the different manufacturing. In particular, FFs strongly depend on the TCO resistivity and on the metallization, which are different for all cells, except for A and D.

4 | RESULTS AND DISCUSSION

4.1 | Electron-selective base contact

The J-V characteristics of the back contact of the cells listed in Table 2 have been measured as a function of temperature, and the activation energy for each cell has been evaluated as explained in Section 3. Then each E_{act} value for each sample has been reported on the curve in Figure 3, and the corresponding ITO work function has been derived. Even though this method can be considered as an indirect evaluation of Φ_{ITO} , it is worth evidencing that the obtained values refer to the ITO work function at the interface with the underlying n-type-doped a-Si:H, which is the value pinning the Fermi level and determining the band bending and contact properties as illustrated in Section 1. Indeed, most of the direct measurements that can be performed on TCO films to determine their work function (for example, Ultraviolet Photoemission Spectroscopy—UPS²²—or Kelvin Probe²³) are referred to the free surface of the TCO layer. Moreover, it is very difficult to evaluate the correct Φ value of air-exposed ITO. It is well-known that environmental contamination can cause an alteration of the ITO work function during the UPS measurements, due to the effects of the ultraviolet (UV) radiation itself.²⁴ Surface cleaning before the measurement does not allow a correct estimation of Φ_{ITO} , either.²⁵ Capacitance-Voltage (C-V) measurement is also an indirect evaluation of the TCO workfunction,²⁶ but it is sometimes too

TABLE 3 Photovoltaic parameters of the complete cells reported in Table 2

Sample	V_{oc} (mV)	J_{sc} (mA/cm ²)	FF (%)	Eff (%)
Cell A	730	37.1	79.5	21.5
Cell B	710	31.1	68.2	15.1
Cell C	693	32.3	61.8	13.8
Cell D	734	37.5	80.3	22.1
Cell E	662	35.2	79.2	18.4

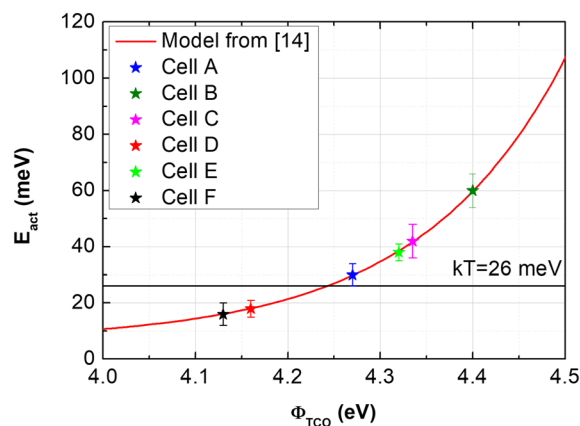


FIGURE 3 Theoretical trend (red curve, taken from our previous work¹⁴) of the activation energy on the base contact E_{act} as a function of the TCO workfunction Φ_{TCO} . The symbols correspond to the E_{act} calculated from experimental measurements on the investigated samples. The black horizontal line represents the 26 meV energy corresponding to room temperature [Colour figure can be viewed at wileyonlinelibrary.com]

sensitive to the defect density at the interface between the TCO and the silicon substrate. Furthermore, the TCO film growth is influenced by several parameters, like the substrate nature and morphology^{27,28} or the layer thickness,²⁹ that can modify the film properties during the growth and, in turn, modify the film work function. Consequently, the mentioned techniques can only assess Φ_{TCO} at the free surface.

Coming back to the results shown in Figure 3, some considerations can be done. The base contacts of cells B, C, and D differ in the sputtering system and deposition temperature of ITO. It can be observed that, in the case of the ITO layer deposited at low temperature (sample B), the activation energy is $E_{\text{act}} = 59.7$ meV, and the resulting work function is the highest (4.4 eV), as expected from the trend reported in the literature.³⁰ On the other hand, the base contacts of cells C and D, where ITO has been deposited at high temperature, are characterized by lower activation energy values (42.4 and 18.5 meV, respectively), with Φ_{TCO} of 4.33 and 4.16 eV, respectively, again in accordance with the trend reported in reference.³⁰ As cells B and C activation energies lie above the 26 meV threshold, they both reveal a barrier at the base contact, evidencing that Φ_{ITO} is not sufficiently low, neither when the ITO is produced at higher temperature. On the other hand, the different system used for depositing the base contact ITO of cell D allows producing a material with such a low work function that the corresponding activation energy lies below the 26 meV threshold line.

Regarding samples E and F, both having the same a-SiOx:H buffer layer, the ITO layers on the base contacts have been grown by RF sputtering at high temperature but in a different deposition system. From the analysis of the cells back contacts, it can be seen that the ITO of sample F is better optimized and produces a low activation energy of 16 meV, corresponding to a $\Phi_{\text{TCO}} = 4.13$ eV.

4.2 | Influence of the Φ_{TCO} at the base contact on FF

Among all the proposed samples, the two cells produced within the European H2020 Ampere project (cells A and D) can be considered as almost identical except for the TCOs deposition conditions, as evident from their light J–V characteristics in Figure 4. Comparing the base contacts of these two cells, we can see that their E_{act} differs only by 11.5 meV, which corresponds to a difference in Φ_{TCO} of 0.12 eV, with the cell A being below the 26 meV threshold reported in Figure 3. Thus, the barriers on the base contacts of the two cells have different behaviors at RT. For this reason, in principle, the FF of cell D should be substantially higher than that of cell A, while actually the cells FFs reported in Table 3 and Figure 4 do not differ much. This can be explained by the considerations described in a previous work,¹⁴ where it is reported that the cell FF variation as a function of the TCO work function is very small for $\Phi_{\text{TCO}} < 4.3$ eV and can be mitigated by the presence of a highly doped amorphous layer. Indeed, the phosphorous concentrations in the amorphous layers of both cells, measured by SIMS profile analysis, are higher than 1×10^{20} at/cm³.

Nevertheless, the light J–V characteristics of Figure 4 show that the cell FFs have not very impressive values, even though for cell D, the base contact issue can be considered as almost absent. To find an explanation to this fact, an analysis focused on the holes collection into the emitter layer is then suggested.

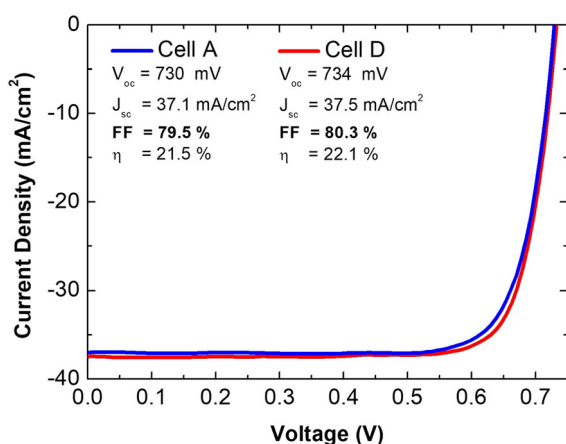


FIGURE 4 Light J–V characteristics and photovoltaic parameters at RT of cells A and D. The fill factors of the cells are highlighted [Colour figure can be viewed at wileyonlinelibrary.com]

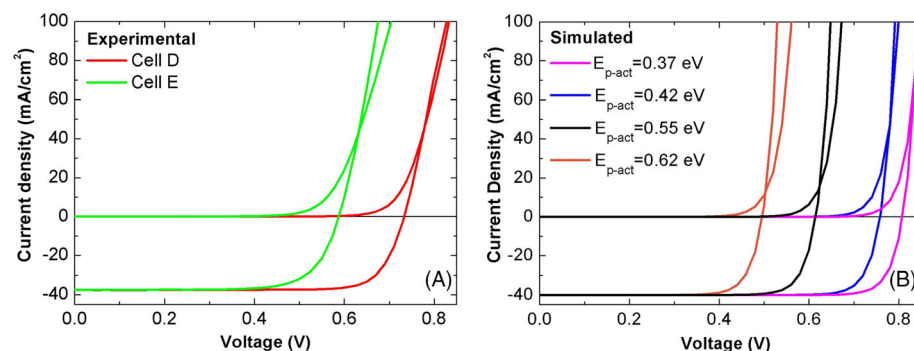


FIGURE 5 Light and dark J–V characteristics at RT of HJ solar cells showing the crossing of the curves. (A) Experimental curves of cells D and E; (B) simulated characteristics of HJ cells having different doping activation energies $E_{\text{p-act}}$. The figures evidence the crossing of all couples of curves [Colour figure can be viewed at wileyonlinelibrary.com]

4.3 | Hole-selective emitter contact

As already mentioned in the introduction, the holes collection takes place at the TCO/(p) a-Si:H/(i) a-Si:H/n-c-Si heterostructure. Here, the contact selectivity is ensured by the electric field that allows the jump over the barrier by thermionic emission. At this interface, the higher the built-in voltage, the better the holes collection. In Figure 1, the band diagram distribution of the complete HJ cell under dark, short circuit and RT conditions is depicted, as deduced from numerical simulations. The blue arrow evidences the jump over the valence band offset that has to be performed by holes. Moreover, it is evident that the c-Si wafer depletes and inverts over the heterointerface due to the doping efficiency of the emitter layer. Therefore, the electric field in the p-type region of the junction is distributed along the c-Si wafer and has a tail into the a-Si:H film, as evidenced from the band bending toward the front contact TCO on the left of Figure 1. The valence band offset ΔE_v represents a limit to thermionic emission: indeed, intuitively, the higher the barrier, the lower the collection probability. As a consequence, such barrier plays a role in the determination of the FF value of the solar cell. Clearly, the impact of the barrier is more evident under illumination, because the holes generated into the n-c-Si absorber must cross the barrier to be collected by the emitter layer and then produce a current available for the external circuit. On the other hand, the role of the valence band offset is less relevant when the cell is in dark conditions and forward bias because of majority carrier injection into the oppositely doped region. Instead such an offset helps reducing the current flow when the cell is reverse biased, if the c-Si surface is perfectly passivated as commonly ensured by a 5-nm-thick intrinsic a-Si:H layer.

Three main issues should be considered when investigating FF limitations due to the emitter side of the HJ cell: (i) the density of defects at the interface (D_{it}), (ii) the valence band energy offset at the emitter side, and (iii) the doping level of the (p) a-Si:H layer, which produces the built-in voltage. By measuring a dark J–V characteristic of a cell it is possible to investigate how the recombination current and the effect of series resistance reduce the current injection and affect the reverse saturation current J_0 . However, this information alone does not help in describing the charge collection mechanism, which determines the cell FF. This suggested to overlap the light and dark J–V curves of several cells, which appeared to be a quick and useful method (described in the following) to extract information about a cell FF limitations.

Under the hypothesis of low defect density at the hetero-interface, in a homojunction cell, the dark and light J–V characteristics do not cross each other in the first quadrant, as expected from the theory of linear overlap of the generation current and the injection current.³¹ Instead, in a HJ cell, the dark characteristic crosses the light one, as clearly evident from experimental measurements and also confirmed by simulations as reported in Figure 5A and 5B, respectively. From Figure 5A, it can be seen that the crossing point takes place at different forward bias voltages for cells D and E. The simulations in Figure 5B reveal that such voltage is strongly dependent on the doping activation energy (E_{p-act}) in the emitter a-Si:H layer, while the corresponding FF values vary between 79% and 85.5%, in accordance with the trend already simulated and reported in reference.¹⁴ Consequently, the lower the E_{p-act} is, the higher the crossing voltage and the V_{oc} of the cell are. When the HJ cell reaches very high V_{oc} values, the crossing between the two curves almost disappears, meaning that the cell is no more affected by any built-in voltage lack due to the valence band offset, that in the simulations is kept at a constant value of 0.45 eV. The crossing disappears for a p-type doped a-Si:H emitter layer with E_{p-act} lower than 0.2 eV. This is in accordance with what shown in Figure 5A, where the V_{oc} and crossing point for cell E lie at lower voltage values than for cell D, since the former cell has been intentionally produced with a lower emitter doping than that of cell D, which comes from an industrial manufacturing line. Even though in practice it is very difficult to achieve a doping value on p-type a-Si:H layer corresponding to an E_{p-act} as low as 0.2 eV, the crossing voltage can be assumed as a useful indication of the overall cell quality, leaving eventual room for further improvements. Of course, a higher valence band offset with respect to the indicated 0.45 eV could produce a stronger limitation to holes collection. In this case, different transport methods, such as tunneling assisted mechanisms or graded energy gap passivation layers, are necessary to overcome the barrier to holes collection. In the simulation of the a-Si:H/c-Si interface, these latter suggested mechanisms are not necessary to describe the experimental evidence.

A confirmation of the valence band offset issue can be further obtained by reducing the working temperature of the solar HJ. Indeed, the presence of a valence band offset at the emitter heterointerface becomes more evident, and its effect can be then better

addressed. As already described,¹⁴ in order to evaluate the temperature effect on the emitter side of the cell alone, the base contact of the samples has been replaced by a perfect ohmic contact (see Section 3.3 for details), since the base contact of the HJ cell is sensitive to the temperature and can, in some cases, affect the overall cell performances. Unfortunately, in this way, also the silicon surface passivation has been removed, but the HJ still acts as a solar cell, even if with limited performances. The light J–V characteristics at different temperatures of the so-obtained hole selective contact for cell D are shown in Figure 6A. At low temperatures, a marked S-shape is evident, which strongly affects the cell FF, while around 240 K a transition to a single diode behavior is seen. Around RT the cell does not show any S-shape. It can be noticed that the cell V_{oc} at 300 K is lower than the value reported in Table 3 and Figure 4, as an effect of the missing passivating contact on the back.

Figure 7 (symbols) collects the FF value at different temperatures of the hole selective contact of cell D shown in Figure 6A, normalized with respect to the RT value; the data show that the FF value reaches

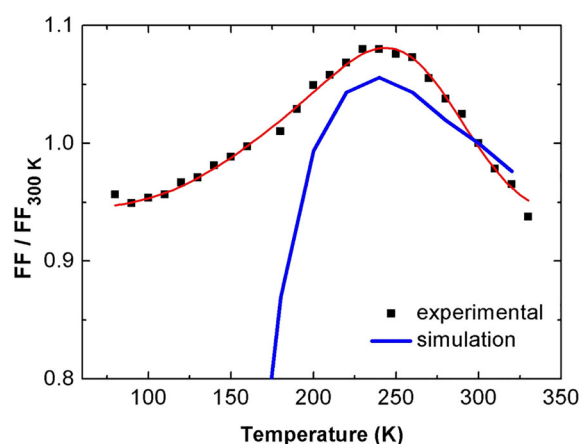


FIGURE 7 Normalized fill factor values at different temperatures of the J–V characteristics reported in Figure 6: the symbols are experimental values referred to cell D (Figure 6A), while the blue line is obtained from the simulated curves of Figure 6C. The red line is a guide for the eye. Both experimental and simulated data show similar trends [Colour figure can be viewed at wileyonlinelibrary.com]

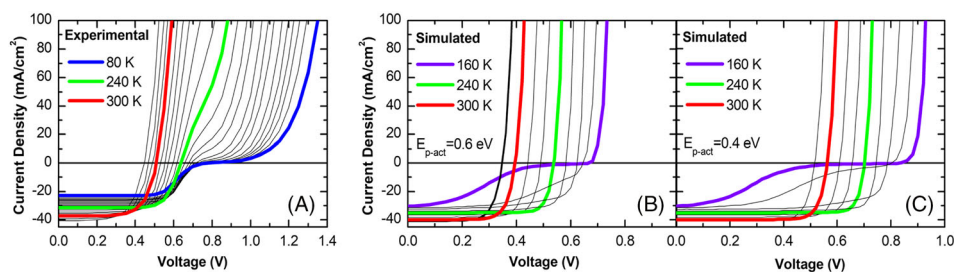


FIGURE 6 Bundles of light J–V characteristics at different temperatures of the hole selective contact of HJ structures having a metallic base contact: (A) experimental data for cell D; (B,C) simulated curves for two HJ solar cells with different doping activation energies E_{p-act} . Both experimental and simulated curves show the appearance of an S-shape at decreasing temperatures [Colour figure can be viewed at wileyonlinelibrary.com]

a maximum around 240 K, which can be seen as the transition temperature toward the S-shape in the J–V characteristics. A structure similar to the one measured in Figure 6A can be simulated as an HJ cell having the base contact modeled as a recombining ohmic contact with InGa. Figure 6B and 6C show the simulated light J–V characteristics at different temperatures for two different E_{p-act} values of 0.6 and 0.4 eV, respectively. The simulations reported in Figure 6B and 6C are quite similar but do not exactly fit the experimental data of Figure 6A. However, they suggest that the J–V bundle lies in different voltage ranges depending on the E_{p-act} , while the S-shape appearance in the J–V curve bundle is due to the valence band offset. Therefore, the numerical simulations are useful to remark that the band offset and the E_{p-act} contribute in different ways to the cell FF issue related to the emitter side.

The blue curve in Figure 7 is derived from the evaluation of the FF of the simulated curve bundle in Figure 6C. The simulated FF trend is quite similar to the experimental one; therefore, it can be deduced that the S-shape seen in the J–V characteristics bundle is only due to the valence band offset, no matter the E_{p-act} value. It is worth noticing that in all simulations a very low D_{it} (10^9 cm^{-2}) at the heterointerface is chosen, in order to exclude the influence of this parameter from the discussion.

As ΔE_v depends on the difference between the energy gap values E_g of c-Si and (p) a-Si:H, and since with decreasing temperature there is a higher enhancement of E_g in the a-Si:H film with respect to the one in the c-Si wafer,^{32,33} the corresponding ΔE_v varies with temperature as shown in Figure 8. Consequently, below 240 K, when ΔE_v increases, the electric field is not sufficient to ensure a complete thermionic emission of holes over that band offset, so that the S-shape appears and the FF is reduced. From the simulated curves in Figure 6B and 6C it is seen that a lower E_{p-act} corresponds to the J–V characteristic bundle shifted to higher voltages, even if the S-shape does not disappear, thus confirming that the barrier is still present even when enhancing the built-in voltage of the cell. These simulations indirectly confirm the hypothesis that the electron affinities of a-Si:H and c-Si negligibly depend on the temperature, letting the valence band offset be the cell parameter which is most affected by

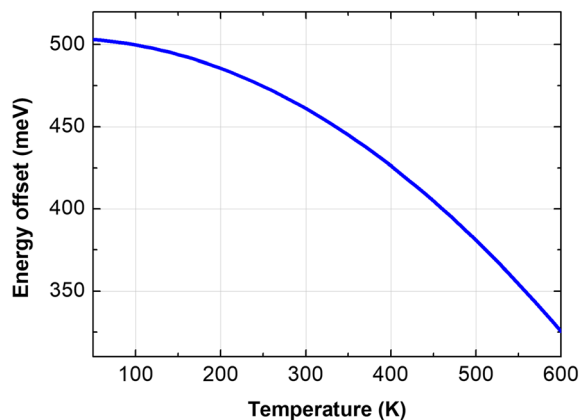


FIGURE 8 Valence band offset as a function of temperature in a a-Si:H/c-Si solar cell [Colour figure can be viewed at [wileyonlinelibrary.com](https://onlinelibrary.wiley.com)]

the working temperature of the device. Finally, it is relevant to remark that the above-described low temperature effect on HJ cells FF does not limit the use of the cells at RT or in the temperature range of common use for HJ solar panels.

5 | CONCLUSIONS

This work, which can be considered as the extension of a previous more theoretical and detailed one,¹⁴ is focused on the investigation of different FF limitations of HJ solar cells coming from barriers arising at both the base and the emitter contacts. Six HJ solar cells were grown with different characteristics; the J–V characteristics of their base and emitter contacts were measured separately and compared with simulated curves.

Regarding the base contact, it is remarked that the work function of the TCO must be carefully optimized in order to obtain a perfect ohmic contact at RT. To this aim, a method to indirectly measure the actual Φ_{TCO} value at the (n) a-Si:H/TCO interface is proposed, which consists of calculating the activation energy E_{act} of the hidden barrier and placing the obtained value on the theoretical curve already shown in a previous work.¹⁴ Even though the method requires measuring the J–V characteristics as a function of temperature, which is not an easy task for large area cells, however it is valid even in a restricted range of temperatures, that is, between 330 and 240 K, which can be easily reached at both laboratory and production line scale even without a specific large area cryogenic system.

FF limitations are also recognized on the emitter contacts, which are evidenced by two features observed on the J–V characteristics. The first is the crossing of the light and dark curves at RT, and it is shown that the higher the voltage at which the crossing happens, the lower the barrier experienced by the carriers. The second is the appearance of a S-shape in the light curves at low temperatures, and it is shown that this effect is only due to the valence band energy offset at the emitter and determines the FF and V_{oc} values of the HJ cell. The effect can be mitigated by increasing the doping level in the (p) a-Si:H, thus reducing the E_{p-act} .

ACKNOWLEDGEMENT

This work has received funding from the European Union's Horizon 2020 research and innovation program under grant agreement No 745601, AMPERE Project.

ORCID

Luca Serenelli  <https://orcid.org/0000-0003-4584-4672>

REFERENCES

- Green MA, Dunlop ED, Hohl-Ebinger J, Yoshita M, Kopidakis N, Ho-Baillie AWY. Solar cell efficiency tables (Version 55). *Prog Photovolt Res Appl*. 2020;28(1):3-15.
- Yoshikawa K, Kawasaki H, Yoshida W, et al. Silicon heterojunction solar cell with interdigitated back contacts for a photoconversion efficiency over 26%. *Nat Energy*. 2017;2(5):17032.

3. Schwartz RJ, Lammert MD. *Silicon Solar Cells for High-Concentration Application*. Washington, DC: IEEE International Electron Devices Meeting; 1975:350-351.
4. Tanaka M, Taguchi M, Kuroda S, et al. Development of new a-Si/c-Si heterojunction solar cells: ACJ-HIT (artificially constructed junction with intrinsic thin-layer). *Jpn J Appl Phys*. 1992;31(11):3518-3522.
5. Tucci M, Serenelli L, Salza E, et al. Innovative design of amorphous/crystalline silicon heterojunction solar cell. *Thin Solid Films*. 2008;516(20):6771-6774.
6. www.enelgreenpower.com/who-we-are/innovation/hjt-photovoltaic-panel
7. <http://taiyangnews.info/technology/25-efficiency-for-heterojunction-solar-cell/>
8. www.pv-magazine.com/2020/02/03/cea-ines-and-enel-announce-24-63-efficiency-for-heterojunction-solar-cell/, 2020.
9. Gerenton F, Harrison S, Eymard J, et al. Silicon heterojunction and half-cell configuration: optimization path for increased module power. *IEEE 46th Photovoltaic Specialists Conference (PVSC)*. 2019;3258-3262.
10. Adachi D, Hernandez JL, Yamamoto K. Impact of carrier recombination on fill factor for large area heterojunction crystalline silicon solar cell with 25.1% efficiency. *Appl. Phys. Lett.* 2015;107:233506-233503.
11. Green MA. Solar cell fill factors: general graph and empirical expression. *Solid State Electron*. 1981;24(8):788-789.
12. Tucci M, Serenelli L, de Iulius S, et al. Contact formation on a-Si:H/c-Si heterostructure solar cells. In: van Sark W, Korte L, Roca F, eds. *Physics and Technology of Amorphous-Crystalline Heterostructure Silicon Solar Cells*, chap 10. Springer. ISBN: 2012:331-375. ISBN:978-3-642-12011-4.
13. Serenelli L, Miliciani M, Izzi M, Chierchia R, Mittiga A, Tucci M. Advances in screen printing metallization for a-Si:H/c-Si heterojunction solar cells. In: *40th IEEE Photovoltaic Specialist Conference*. Denver, CO; 2014:2526-2532.
14. Martini L, Serenelli L, Menchini F, Izzi M, Tucci M. Silicon heterojunction solar cells toward higher fill factor. *Prog Photovolt Res Appl*. 2020;28(4):307-320.
15. Reusch M, Bivour M, Hermle M, Glunz S. Fill factor limitation of silicon heterojunction solar cells by junction recombination. *Energy Procedia*. 2013;38:297-304.
16. Centurioni E, Iencinella D. Role of front contact work function on amorphous silicon/crystalline silicon heterojunction solar cell performance. *IEEE Electron Device Letters*. 2003;24(3):177-179.
17. Dhar A, Ahmad G, Pradhan D, Roy JN. Performance analysis of c-Si heterojunction solar cell with passivated transition metal oxides carrier-selective contacts. *J Comput Electron*. 2020;19(2):875-883.
18. Tomasi A, Sahli F, Seif JP, et al. Transparent electrodes in silicon heterojunction solar cells: influence on contact passivation. *IEEE Journal of Photovoltaics*. 2016;6(1):17-27.
19. Tucci M, de Cesare G. 17% efficiency heterostructure solar cell based on p-type crystalline silicon. *J Non Cryst Solids*. 2004;338(1):663-667.
20. Danel A, Harrison S, Gérenton F, et al. Silicon heterojunction solar cells with open-circuit-voltage above 750mV. In: *Proc. of the 35th European Photovoltaic Solar Energy Conference and Exhibition*. Brussels, Belgium; 2018:444-447.
21. Serenelli L, Martini L, Imbimbo L, et al. Metastability of a-SiOx:H thin films for c-Si surface passivation. *Appl Surf Sci*. 2017;392:430-440.
22. Park Y, Choong V, Gao Y, Hsieh BR, Tang CW. Work function of indium tin oxide transparent conductor measured by photoelectron spectroscopy. *Appl Phys Lett*. 1996;68(19):2699-2701.
23. Ishida T, Kobayashi H, Nakato Y. Structures and properties of electron-beam-evaporated indium tin oxide films as studied by x-ray photoelectron spectroscopy and work-function measurements. *J Appl Phys*. 1993;73(9):4344-4350.
24. Schlaf R, Murata H, Kafafi ZH. Work function measurements on indium tin oxide films. *Journal of Electron Spectroscopy and Related Phenomena*. 2001;120(1-3):149-154.
25. Sugiyama K, Ishii H, Ouchi Y, Seki K. Dependence of indium-tin-oxide work function on surface cleaning method as studied by ultraviolet and x-ray photoemission spectroscopies. *J Appl Phys*. 2000;87(1):295-298.
26. Schroder DK. *Semiconductor Material and Device Characterization*. 3rd ed. New Jersey: Wiley & Sons; 2006.
27. Manavizadeh N, Boroumand FA, Asl-Soleimani E, et al. Influence of substrates on the structural and morphological properties of RF sputtered ITO thin films for photovoltaic application. *Thin Solid Films*. 2009;517(7):2324-2327.
28. Li C, Furuta M, Matsuda T, Hiramatsu T, Furuta H, Hirao T. Effects of substrate on the structural, electrical and optical properties of Al-doped ZnO films prepared by radio frequency magnetron sputtering. *Thin Solid Films*. 2009;517(11):3265-3268.
29. Damiani LR, Mansano RD. Thickness dependence of indium-tin oxide thin films deposited by RF magnetron sputtering. *ECS Transactions*. 2010;31(1):117-124.
30. Klein A, Körber C, Wachau A, et al. Surface potentials of magnetron sputtered transparent conducting oxides. *Thin Solid Films*. 2009;518(4):1197-1203.
31. Green MA. *Solar Cell: Operating Principles, technology and System Applications*. the University of New South Wales, Photovoltaics Centre; 1998.
32. Weiser G, Mell H. Temperature dependence of the optical absorption edge in a-Si:H. *J Non Cryst Solids*. 1989;114:298-300.
33. Priyanka S, Ravindra NM. Temperature dependence of solar cell performance—an analysis. *Solar Energy Materials & Solar Cells*. 2012;101:36-45.

How to cite this article: Serenelli L, Martini L, Menchini F, et al. Selective contacts and fill factor limitations in heterojunction solar cells. *Prog Photovolt Res Appl*. 2021;1–9. <https://doi.org/10.1002/pip.3418>